Implementation of energy and gradient for the TDDFT- approximate auxiliary function (aas) method

Yuchen Wang, Shana Havenridge, and Christine M. Aikens*

Department of Chemistry, Kansas State University, Manhattan, KS 66506, USA

*Email: cmaikens@ksu.edu

Abstract

In this work, we have implemented the time-dependent density functional theory approximate auxiliary (TDDFT-aas) method, which is an approximate TDDFT method. Instead of calculating the exact two-center electron integrals in the *K* coupling matrix when solving the Casida equation, we approximate the integrals, thereby reducing the computational cost. In contrast to the related TDDFT+TB method, a new type of gamma function is used in the coupling matrix that does not depend on the tight binding parameters. The calculated absorption spectra of silver and gold nanoparticles using TDDFT-aas shows good agreement with TDDFT and TDDFT+TB results. In addition, we have implemented the analytical excited-state gradients for the TDDFT-aas method, which makes it possible to calculate the emission energy of molecular systems.

Introduction

Time-dependent density functional theory (TDDFT) has been successfully applied for the calculation of excited-state properties for small molecule, biomolecule, nanocluster, and solid-state systems. [1–4] TDDFT is built on DFT; however, since the classic Hohenberg-Kohn formulation of density functional theory is time-independent, DFT itself is not used for the excited state problem. Runge and Gross extended the theorem to excited states by incorporating a time-dependent external potential into the Hohenberg-Kohn DFT formalism. [5] Casida then formulated the linear-response formalism of solving a time-dependent DFT equations, where the electron density experiences a linear response to an external potential perturbation. [6,7] In practice, the linear-response formalism is sufficient to calculate the excitation spectrum of the system in response to a weak perturbation. The Casida formalism for TDDFT to solve for the excitation

energies has been implemented in a variety of quantum chemistry calculation codes to calculate absorption spectra for systems of interest.

As the size of the system increases, the computational time and memory increase significantly for TDDFT calculations, in part because the coupling matrix requires calculation of many two-electron integrals. Recently, some approximation methods to TDDFT have been proposed to reduce the computational cost, such as TD-DFTB (time-dependent density functional tight binding), [8,9] sTDDFT (simplified TDDFT), [10] sTDA (simplified Tamm-Dancoff approximation), [11,12] TDDFT+TB (TDDFT plus tight-binding), [13] TDDFT-as (TDDFT using auxiliary basis function s), [14] TDDFT-ris (TDDFT with resolution of the identity and auxiliary basis function s), [15] and polTDDFT [16] which we will briefly review. TD-DFTB is a linear response formulation of the semiempirical density functional tight-binding method. In this method, the ground state calculations use trial densities instead of using actual densities. The trial density is a superposition of atomic contributions and needs to be parameterized. In general, DFTB calculations incorporate many parameters that must be determined in advance for each pair of atoms. [17,18] For TD-DFTB excited-state calculations, the K coupling matrix is calculated by using an approximation $K_{ia,jb} = \sum_{AB}\ q_{ia,A}\gamma_{AB}q_{jb,B}$ where q represents transition charges from a Mulliken population analysis, and the γ_{AB} function depends on the distance between two atoms A and B (R_{AB}) and chemical hardness parameters for each element. To avoid the need for extensive parameterization required for ground-state DFTB, several recent methods have combined aspects of DFT and DFTB. For sTDA and sTDDFT, standard DFT is employed for the ground state calculations, and therefore, an approximation is only used in the excited state calculation. TDDFT+TB is motivated by sTDA and sTDDFT as it also uses standard DFT for the ground state calculations. For these excited-state calculations, the coupling matrix is calculated using the same equation as TD-DFTB, although Löwdin population analysis is used to calculate the q. Compared with sTDA and sTDDFT, TDDFT+TB does not take the Hartree-Fock exchange term into account when doing the approximations, which makes TDDFT+TB only applicable to pure functionals. Because the excited-state calculations are based on the actual density obtained from DFT calculations, TDDFT+TB achieves more accurate results compared with TD-DFTB. By using this approximation, TDDFT+TB can address the computational limitations of calculating large molecules and nanoparticles. [19–22] The TDDFT-as method is similar to TDDFT+TB. Both of

these methods approximate the K coupling matrix when solving the linear Casida equation. However, in the TDDFT-as method the γ_{AB} function is only dependent on the distance between two atoms A and B (R_{AB}), and only a single orbital exponent needs to be varied. Moreover, TDDFT-as calculates the transition densities rather than using a Mulliken or Löwdin approximation. TDDFT-as has shown success in calculating absorption spectra specifically for silver nanoparticles. [14] The TDDFT-ris method is an extension to the TDDFT-as method, where the exponent in γ_{AB} is related to the element types in the system. In addition, TDDFT-ris takes the Hartree-Fock exchange terms into account. [14] For polTDDFT, the method simplifies the algorithm by avoiding the Davidson diagonalization and applying a resolution of identity scheme, thereby saving calculation time, and the method has shown successful application in studying the optical properties of metal nanoclusters. [23,24]

Linear-response TDDFT calculations provide vertical excitation information that can be used to produce absorption spectra. To elucidate other optical properties such as photo-catalytic reaction pathways or photoluminescence, it is important to understand the excited state potential energy surface. Thus, gradient calculations (which are required for excited-state geometry optimizations) are needed to explore the potential energy surface and study these optical properties. However, using TDDFT to perform excited-state gradient calculations is computationally expensive. Recently, the analytical gradient of the TDDFT+TB method has been derived, which enables speeding up the excited-state geometry optimization process. [25]

In this work, we develop a new TDDFT approximation method called TDDFT-aas (TDDFT- approximate auxiliary s function). The method resembles both the TDDFT+TB and TDDFT-as methods. The K coupling matrix is calculated using $K^{S}_{ia,jb} = \sum_{AB}\ q_{ia,A}\gamma_{AB}q_{jb,B}$, the Löwdin population analysis is used for q, and the γ_{AB} function is used from the TDDFT-as method. Thus, the TDDFT-aas method is independent of chemical hardness parameters. After implementing the TDDFT-aas excitation energy, we examine the absorption spectra for a variety of gold/silver nanoclusters. In addition to the energy calculation, we also implement the gradient for the TDDFT-aas method. The gradient calculation enables us to complete TDDFT-aas excited state geometry optimizations to calculate radiative emission energies. After derivation and implementation of the TDDFT-aas energy and gradient, numerical and analytical gradients are calculated and compared to examine the accuracy of the analytical gradient. Emission energies for

systems ranging from diatomic molecules to gold thiolate-stabilized nanoclusters are calculated. Lastly, we compare the computational costs between different approximation methods. Overall, because TDDFT-aas does not require tight-binding parameters, the method is easier to implement compared with other semi-empirical approximation methods.

Theory and code implementation

The linear formalism of TDDFT within the Casida approach [6,7] can be written starting with equation 1:

$$\begin{pmatrix} \mathbf{A} & \mathbf{B} \\ \mathbf{B}^* & \mathbf{A} \end{pmatrix} \begin{pmatrix} \mathbf{X} \\ \mathbf{Y} \end{pmatrix} = \omega \begin{pmatrix} 1 & 0 \\ 0 & -1 \end{pmatrix} \begin{pmatrix} \mathbf{X} \\ \mathbf{Y} \end{pmatrix} \quad (1)$$

where **A** and **B** represent rotational Hessian matrices and ω represents the excitation energy. **X** and **Y** are eigenvectors that correspond to the excitation and deexcitation respectively. The linear Casida equation can be transformed into the formalism of $\mathbf{\Omega F} = \omega^2 \mathbf{F}$, where $\mathbf{F} = (\mathbf{A} - \mathbf{B})^{-\frac{1}{2}}(\mathbf{X} + \mathbf{Y})$ and $\mathbf{\Omega} = (\mathbf{A} - \mathbf{B})^{\frac{1}{2}}(\mathbf{A} + \mathbf{B})(\mathbf{A} - \mathbf{B})^{\frac{1}{2}}$. [6] To solve the equation, $\mathbf{A} + \mathbf{B}$ and $\mathbf{A} - \mathbf{B}$ need to be calculated. The matrices have the following formulas:

$$A_{ia,jb} + B_{ia,jb} = \delta_{ab}\delta_{ij}(\epsilon_a - \epsilon_i) + 2(ia \mid jb) + 2(ia|f_{xc}|jb) - a_x((ij \mid ab) + (ib \mid ja) \quad (2)$$

$$A_{ia,jb} - B_{ia,jb} = \delta_{ab}\delta_{ij}(\epsilon_a - \epsilon_i) - a_x((ij \mid ab) - (ib \mid ja)) \quad (3)$$

where *i, j* represent occupied orbitals and *a, b* represent virtual orbitals; $(\epsilon_a - \epsilon_i)$ represents the orbital energy difference between orbital index *i* and *a;* a_x is the amount of Hartree-Fock exchange; and $(ia \mid jb)$ and $(ia|f_{xc}|jb)$ are the usual two-electron integrals. If we only consider pure functionals, a_x = 0 and therefore $\mathbf{A} + \mathbf{B}$ and $\mathbf{A} - \mathbf{B}$ can be reduced to:

$$A_{ia,jb} + B_{ia,jb} = \delta_{ab}\delta_{ij}(\epsilon_a - \epsilon_i) + 2(ia \mid jb) + 2(ia|f_{xc}|jb) \quad (4)$$

$$A_{ia,jb} - B_{ia,jb} = \delta_{ab}\delta_{ij}(\epsilon_a - \epsilon_i) \quad (5)$$

TDDFT-aas makes the same approximation as TDDFT+TB, where the exact two-center electron integrals calculations are approximated. In this way, instead of calculating the integrals $(ia \mid jb)$ and $(ia|f_{xc}|jb)$, the approximation $K_{ia,jb} = \sum_{AB} q_{ia,A}\gamma_{AB}q_{jb,B}$ is used, where *A* and *B* are the two nuclei from which the two-center integrals arise, and *q* represents transition charges from a Löwdin population analysis that can be written as $q_{ia,A} = \sum_{\mu \in A} C'_{\mu i}C'_{\mu a}$, where $C' = S^{1/2}C$.

In this equation, C represents the coefficient matrix of the Kohn-Sham orbitals; μ, ν, κ, and λ indicate atomic basis functions; and $S^{1/2}$ denotes the square root of the overlap matrix. Though using Löwdin population analysis can have difficulties when using basis sets with diffuse functions, it is somewhat improved compared to Mulliken population analysis. [13] The γ_{AB} function in TDDFT+TB depends on both the distance between two atoms A and B (R_{AB}) and the chemical hardness for each element.

The TDDFT-as method also approximates the two-center integrals, although it uses the following equation: [14]

$$(ia \mid jb) \approx \sum_{\mu\nu} \sum_{\kappa\lambda} C_\mu^i C_\nu^a C_\kappa^j C_\lambda^b \sum_{PQ} \Delta_{\mu\nu}^A (A \mid B) \Delta_{\kappa\lambda}^B = \sum_{AB} \Gamma_{ia}^A (A \mid B) \Gamma_{jb}^B \quad (6)$$

where

$$\Gamma_{ia}^A = \sum_{\mu\nu} C_\mu^i C_\nu^a \sum_B (A \mid B)^{-1} (B \mid \mu\nu) \quad (7)$$

$$(A \mid B) \approx \gamma(R_{AB}) = \frac{\mathrm{erf}(R_{AB}\sqrt{\alpha/2})}{R_{AB}} \quad (8)$$

For the TDDFT-aas method, we use the same γ_{AB} function as in TDDFT-as method, where $\gamma(R_{AB}) = \frac{\mathrm{erf}(R_{AB}\sqrt{\alpha/2})}{R_{AB}}$, and α is a parameter that needs to be tuned before using the method. In our code, the α value can be selected by the user at runtime. A summary of the differences in the coupling matrix for these three approximation methods is shown in Table 1.

Table 1. Comparison of the TDDFT+TB, TDDFT-as and TDDFT-aas methods.

	TDDFT+TB	TDDFT-as	TDDFT-aas
Coupling matrix	$K_{ia,jb} = \sum_{AB} q_{ia,A} \gamma_{AB} q_{jb,B}$		
Atomic transition charges ($\boldsymbol{q}$)	Löwdin	Equation 7	Löwdin
Gamma function ($\boldsymbol{\gamma_{AB}}$)	$\gamma(R_{AB}) = \gamma_{AB}(\eta_A, \eta_B, R_{AB})$	$\gamma(R_{AB}) = \frac{\mathrm{erf}(R_{AB}\sqrt{\alpha/2})}{R_{AB}}$	

To implement the excited state gradient of the TDDFT-aas method, we start with the full analytical gradient equation for TDDFT+TB, [25] where the equation can be written as:

$$\frac{d\mathrm{E}}{dR_A} = 2\sum_{\mu\in A,\nu\notin A}\frac{dh_{\mu\nu}}{dR_A}P_{\mu\nu} + 2\sum_{\mu,\lambda\in A,\nu,\kappa\notin A}\frac{d(\mu\nu|\lambda\kappa)}{dR_A}P_{\mu\nu}$$
$$+2\sum_{\mu\in A,\nu\notin A}\frac{dV_{\mu\nu}^{XC}}{dR_A}P_{\mu\nu} + 2\sum_{\mu\in A,\nu\notin A}S_{\mu\nu}^{1/2}\frac{dS_{\mu\nu}^{1/2}}{dR_A}(\Xi_A+\Xi_B)U_{\mu\nu} \qquad (9)$$
$$+4\sum_{\mu\in A,\nu\notin A}\frac{d\gamma_{AB}}{dR_A}U_AU_B - \sum_{\mu\in A,\nu\notin A}\frac{dS_{\mu\nu}}{dR_A}W_{\mu\nu}.$$

where $U_A = \sum_{ia}(X+Y)_{ia}q_{ia,A}$ and $\Xi_A = \sum_B \gamma_{AB}U_B$. From the gradient equation, the fourth and fifth terms involve the γ_{AB} function. Because the only difference between TDDFT+TB and TDDFT-aas is the form of γ_{AB}, we can use Equation 9 as the general TDDFT-aas gradient equation and adjust the new equation for the γ_{AB} related terms. We then also derive $\frac{d\gamma_{AB}}{dR_A}$:

$$\frac{d\gamma_{AB}}{dR_A} = \frac{d\gamma_{AB}}{dR_{AB}} * \frac{dR_{AB}}{dR_A} = \frac{\sqrt{\frac{2\alpha}{\pi}}*e^{-R_{AB}^2\frac{\alpha}{2}}*R_{AB} - \left(\mathrm{erf}\left(R_{AB}\sqrt{\frac{\alpha}{2}}\right)\right)}{(R_{AB})^2} * \frac{R_A-R_B}{R_{AB}} \qquad (10)$$

where dR_A represents the change with respect to one coordinate of atom A (x_A, y_A, or z_A), and R_{AB} represents the distance between two atoms A and B.

We have implemented the TDDFT-aas code in the Amsterdam Modeling Suite (AMS), [26] based on the TDDFT+TB gradient code. AMS versions including the TDDFT-aas method can be found at https://www.scm.com/support/downloads/development-snapshots/ with revision numbers equal to or higher than 121656.

Results and discussion

To validate the accuracy of the TDDFT-aas method energies and gradients, we performed test calculations using both linear-response TDDFT energy calculations and excited state geometry optimizations. All of the calculations were completed in a development version of the Amsterdam Density Functional (ADF) engine in the Amsterdam Modeling Suite (AMS). [26]

Optimized tuning parameter

Similar to the TDDFT-as method, the exponent (α) in γ_{AB} needs to be optimized before using the TDDFT-aas method. To tune the α parameter, optical absorption spectra were calculated for the Ag_{20} and Au_{20} tetrahedral nanoclusters with a range of different α values (0.16, 0.18, 0.2, 0.22, 0.24), and the absorption spectra results are plotted and shown in Figure 1. Unless otherwise noted, the Perdew-Burke-Ernzerhof (PBE) [27] exchange correlation functional was used with an all-electron double-zeta (DZ) basis set [28] for the TDDFT-aas calculations of absorption spectra. TDDFT and TDDFT+TB results calculated at the PBE/DZ level of theory are also included in the

absorption spectra for comparison. In all cases, the overall shape of the spectrum and the approximate peak locations are well reproduced for all of the approximate methods. For the Ag_{20} nanocluster, the TDDFT-aas spectra show the best correlation with TDDFT results when α is around 0.2, so α=0.2 is chosen as the default optimized value. The choice of α=0.2 also works well for the Au_{20} nanocluster. For the Ag_{20} nanocluster, the TDDFT-aas methods provide a closer approximation to the TDDFT oscillator strengths than the TDDFT+TB method; this is reversed for the Au_{20} nanocluster.

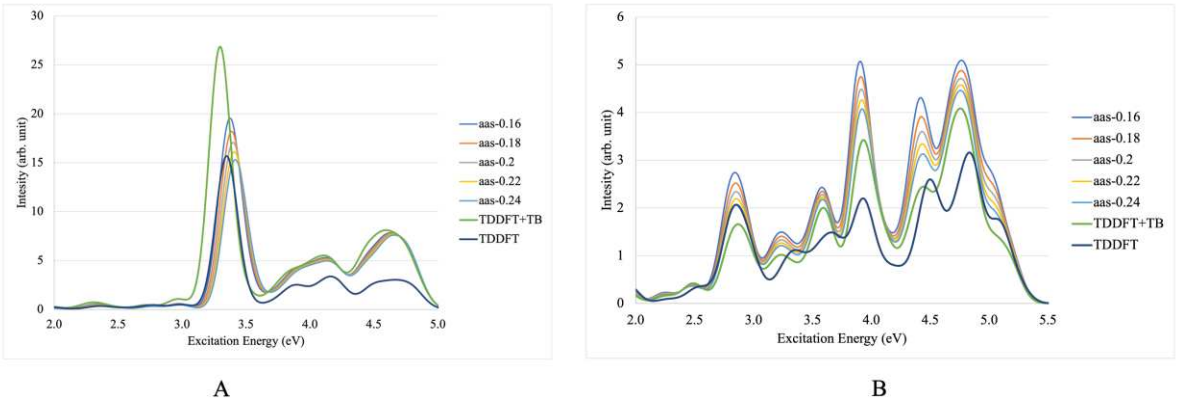

Figure 1. Absorption spectra for tetrahedral clusters A. Ag_{20} and B. Au_{20} calculated by the TDDFT-aas method with different α values. TDDFT and TDDFT+TB calculation results are included for comparison. The spectra were broadened using Gaussian broadening with full width at half-maximum (FWHM) = 0.2 eV.

Comparison of methods for nanocluster absorption spectra

After examining the α parameter dependence for Ag_{20} and Au_{20}, we used 0.2 as the α value to calculate the absorption spectra for representative pure gold (Figure 2) and silver (Figure 3) nanoclusters. The absorption spectra results for the Au_{38}^{+4} system show that both the TDDFT-aas and TDDFT+TB methods underestimate the absorption intensity at around 2.5 eV and overestimate the absorption intensity at around 2.7 eV. For the excitation at around 2.7 eV, both TDDFT-aas and TDDFT+TB show a slight redshift in the excitation energy. From the spectra with a Gaussian broadening, it is hard to observe the peak around 2.5 eV in TDDFT-aas and TDDFT+TB compared with TDDFT results. Stick spectra are shown in the supporting information to better visualize each distinct excitation (Figure S1); in general, the stick spectra have peaks in similar energy ranges, although the TDDFT-aas method predicts more splitting. For the Au_{55}^{+5} system, TDDFT-aas and TDDFT+TB show similar line shapes for their spectra, and they both

underestimate the absorption intensities for excitation at around 1.8 eV and 2.5 eV compared with TDDFT results. The excitation at around 2.1 eV is not apparent in the two approximation methods but can be visualized more clearly from the stick spectra (Figure S2). In summary, TDDFT-aas spectra show very similar line shapes to the TDDFT+TB spectra, and both agree with the excitation energies from TDDFT calculations well but have some issues when predicting the oscillator strengths.

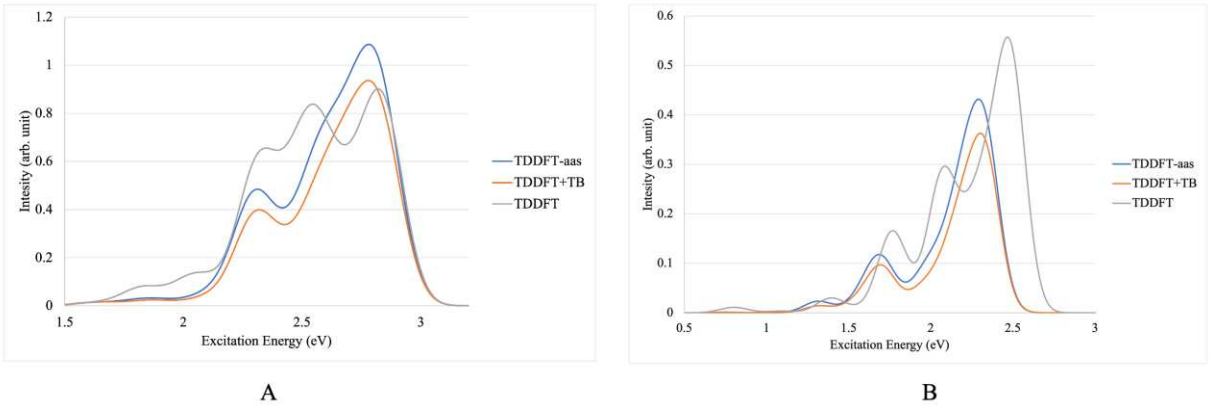

Figure 2. Comparison of the absorption results using TDDFT-aas and TDDFT+TB for pure gold nanoclusters. A. Au_{38}^{+4} B. Au_{55}^{+5} The spectra were broadened using Gaussian broadening with full width at half-maximum (FWHM) = 0.2 eV.

The calculated spectra for representative silver nanoclusters are shown in Figure 3. For the Ag_{38}^{+4} system, the overall spectral line shapes show good agreement among TDDFT, TDDFT+TB, and TDDFT-aas results. TDDFT+TB shows an overestimate of the absorption intensity and redshift of the excitation energy for peaks at around 3.6 eV and 4.0 eV. TDDFT-aas shows relatively better agreement with TDDFT for both excitation energy and absorption intensity compared with TDDFT+TB. For the Ag_{55}^{+5} system, TDDFT-aas slightly underestimates the intensity for the peak located around 3.3 eV and TDDFT+TB overestimates the intensity for that peak compared with the TDDFT results. For the shoulder peak located around 2.9 eV, both two approximation methods show slight blueshifts compared with TDDFT.

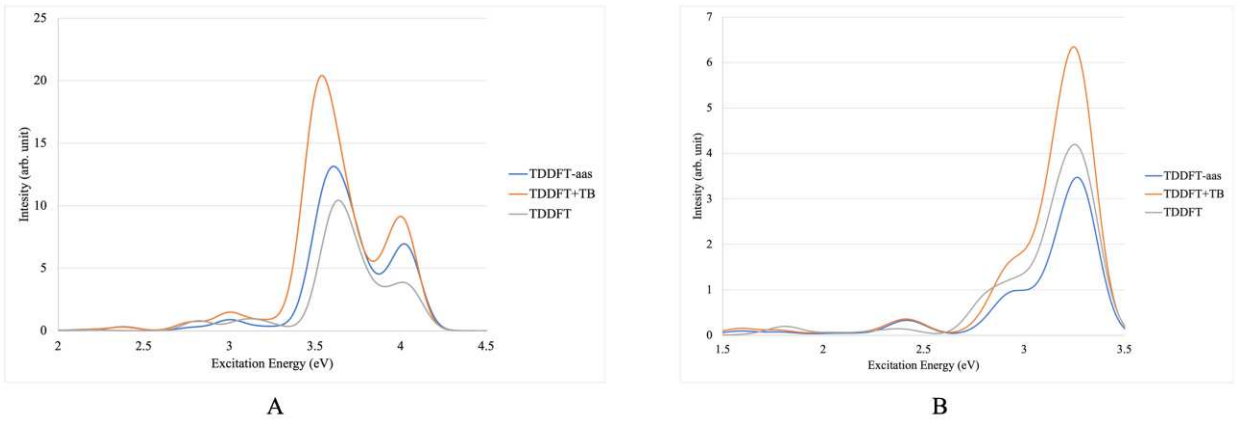

Figure 3. Comparison of the absorption results using TDDFT-aas to calculate pure gold nanoclusters. A. Ag_{38}^{+4} B. Ag_{55}^{+5} The spectra were broadened using Gaussian broadening with full width at half-maximum (FWHM) = 0.2 eV.

Besides the pure metal nanoclusters, the absorption spectra of gold thiolate-protected nanoclusters were also calculated using the TDDFT-aas method, and the calculated spectra and comparison between TDDFT+TB and TDDFT results are shown in Figure 4. Overall, TDDFT-aas shows good agreement with TDDFT for the excitation energies, while it slightly underestimates the oscillator strength of the first absorption peak. For the $Au_{25}(SCH_3)_{18}^-$ system, TDDFT-aas and TDDFT+TB overestimate the oscillator strength of the peak ranges between 3 eV and 4 eV. For the $Au_{38}(SCH_3)_{24}$ system, TDDFT-aas shows good agreement with the peaks around 2.5 eV and overestimates the oscillator strength of the peaks between 2.8 eV and 3.5 eV. Because α is set to be 0.2 for the system, which affects the S, C, and H atoms as well as Au, the absorption spectra results indicate that a generalized α is reasonable for these gold thiolate-protected nanocluster calculations. Overall, systems with less symmetry such as $Au_{25}(SCH_3)_{18}^-$ and $Au_{38}(SCH_3)_{24}$ provide a better match between the approximate TDDFT-aas and TDDFT+TB methods and the original TDDFT method compared to the pure nanoclusters such as Au_{38}^{+4} and Au_{55}^{+5}. This is likely due to the semiempirical approximations inherent in the methods, which reduce the number of integrals calculated, especially for highly symmetric systems. [13]

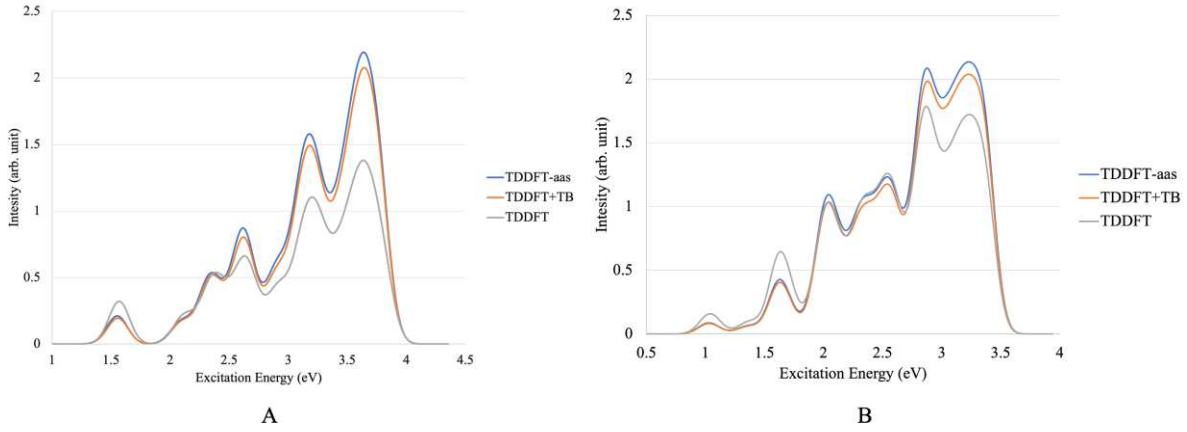

Figure 4. Comparison of the absorption results using TDDFT-aas to calculate thiolate-protected gold nanoclusters. A. $Au_{25}(SCH_3)_{18}^-$ B. $Au_{38}(SCH_3)_{24}$ (α=0.2 is applied for TDDFT-aas calculations) The spectra were broadened using Gaussian broadening with full width at half-maximum (FWHM) = 0.2 eV.

In addition to the PBE functional, the BP86 functional [29,30] was also applied to test the accuracy of TDDFT-aas calculations, and the results are shown in Figure S3. The trends are similar to the PBE calculated results, where TDDFT-aas results show a very similar line shape with TDDFT+TB results; these methods overestimate the oscillator strength of peaks between 3.0 eV and 4.5 eV compared with TDDFT results but achieve very good agreement in excitation energies. The same α value was applied and achieved good agreement for both PBE and BP86 functionals in this work, but users may want to perform a test of α values if they are using very different functionals.

Overall, for the absorption spectra calculations, TDDFT-aas can obtain very similar results to TDDFT+TB calculations, and its excitation energies show good agreement with TDDFT. However, both approximate methods have some artifacts when predicting the oscillator strength.

Numerical and analytical gradients

As discussed in equations 6 and 7, the analytical gradients for TDDFT-aas have been derived in this work. To validate the TDDFT-aas gradient code implementation, we computed numerical and analytical gradients for selected systems and examined the results. For the numerical gradient, a finite difference is used with a step size of 0.001 Å in x, y, and z directions. The MAD (Mean Absolute Deviation) and RMS (Root Mean Square) results between the numerical and analytical gradient were calculated and are shown in Table 2. All MAD values are

smaller than 6.33×10^{-4} Hartree/Å and all RMS values are smaller than 8.15×10^{-4} Hartree/Å. These errors are similar to those for TDDFT+TB and TDDFT. [25] The results demonstrate the accuracy of the TDDFT-aas analytical gradient.

Table 2. Numerical vs. analytical gradient differences (Hartree/Å) for representative molecular systems.

	MAD	RMS
H_2	2.47×10^{-5}	4.22×10^{-5}
Li_2	1.50×10^{-5}	2.11×10^{-5}
N_2	2.11×10^{-4}	3.66×10^{-4}
Cl_2	1.87×10^{-5}	2.45×10^{-5}
HCl	1.66×10^{-5}	2.76×10^{-5}
Uracil	8.25×10^{-5}	1.11×10^{-4}
Ethene	1.23×10^{-4}	2.27×10^{-4}
Acetamide	1.53×10^{-4}	2.20×10^{-4}
Acetone	8.05×10^{-5}	1.39×10^{-4}
Adenine	7.27×10^{-5}	1.04×10^{-4}
Benzoquinone	2.94×10^{-5}	5.62×10^{-5}
Benzene	1.30×10^{-5}	2.53×10^{-5}
Butadiene	2.95×10^{-5}	4.54×10^{-5}
Pyrazine	4.00×10^{-5}	7.14×10^{-5}
Cyclopentadiene	6.33×10^{-4}	8.15×10^{-4}
Cyclopropene	1.87×10^{-4}	2.41×10^{-4}
Cytosine	6.73×10^{-5}	8.35×10^{-5}
Formaldeyde	2.86×10^{-5}	5.20×10^{-5}
Furan	2.56×10^{-5}	3.45×10^{-5}
Hexatriene	1.62×10^{-4}	2.24×10^{-5}
Imidazole	6.27×10^{-5}	1.02×10^{-5}
Pyrimidine	4.46×10^{-5}	8.28×10^{-5}
Pyridazine	5.39×10^{-5}	9.99×10^{-5}
Norbornadiene	2.42×10^{-5}	3.31×10^{-5}
Octatetraene	5.76×10^{-5}	2.12×10^{-4}
Naphthalene	2.05×10^{-5}	3.49×10^{-5}
Thymine	7.45×10^{-5}	9.45×10^{-5}
Triazine	7.33×10^{-5}	9.48×10^{-5}

Excited state geometry optimization

Excited state geometry optimizations were then performed to evaluate the quality of the calculated emission energies. First, we perform excited-state geometry optimizations on several diatomic molecule systems at the PBE/TZP [28] level of theory, and the results are shown in Table 3 and Table S1. Diatomic molecules are known to be a challenging test case for approximate TDDFT methods due to the atomic transition charges' inability to model local transitions; [13] though a useful test of inherent errors, these approximate methods are not required for diatomic molecules because the standard TDDFT method is applicable for these systems.

Table 3. Emission energy for five diatomic molecules (unit: eV) calculated at different level of theories; TDDFT did not calculate an emission energy for H_2 because of its dissociative potential energy surface.

	TDDFT	TDDFT-aas	TDDFT+TB
H_2	N/A	5.80	8.07
Li_2	1.85	1.98	1.60
N_2	6.45	6.97	6.97
Cl_2	1.19	0.94	0.94
HCl	1.71	1.51	1.51

For N_2, Cl_2, and HCl, TDDFT-aas and TDDFT+TB give the same emission energy results, where the energy difference between TDDFT-aas and TDDFT ranges from 0.20 eV to 0.52 eV. The TDDFT-aas method provides identical results to the TDDFT+TB method in these cases. To understand the H_2 and Li_2 cases, potential energy surfaces (PES) for these systems are plotted and shown in Figure 5.

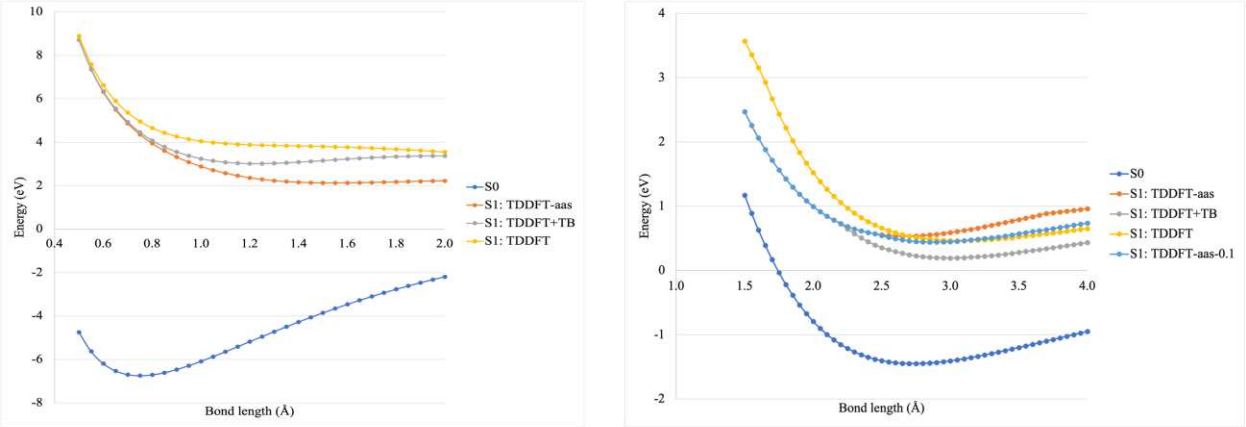

Figure 5 Potential energy surfaces for the A. H_2 and B. Li_2 systems. In the key, S0 represents the PES for the ground state. S1: TDDFT-aas represents the PES for the S_1 state using TDDFT-aas methods with α=0.2. S1: TDDFT-aas-0.1 represents the PES for the S_1 state using TDDFT-aas methods with α=0.1. S1: TDDFT+TB represents the PES for the S_1 state using TDDFT+TB methods. S1: TDDFT represents the PES for the S_1 state using TDDFT methods.

For the S_1 state, TDDFT did not calculate a minimum in the first excitation energy for H_2. The results agree with the reported potential energy surface for H_2, [31] in which there is not a local minimum for the S_1 state. Meanwhile, TDDFT+TB predicts a fairly shallow S_1 minimum

geometry with an H-H bond length of 1.21 Å at 8.07 eV above the ground state energy. TDDFT-aas predicts a very shallow S_1 minimum geometry at an H-H bond distance of 1.53 Å, with an energy of 5.80 eV above the ground state energy. Both of these two methods show long H-H distances for the S_1 minimum, which agree with the dissociative nature of the S_1 potential energy surface.

For Li_2, the S_1 state minima are calculated at 1.85 eV, 1.60 eV, and 1.98 eV for the TDDFT, TDDFT+TB, and TDDFT-aas(α=0.2) methods, respectively. From the PES, TDDFT+TB, and TDDFT-aas (for both α=0.2 and α=0.1) show the same S_1 PES when the Li-Li bond length is less than 2.2 Å; with the increased bond length, TDDFT-aas shows a higher potential energy surface than TDDFT+TB, and the TDDFT-aas PES crosses the TDDFT PES. The higher S_1 PES leads to a change in the order of the excited state compared with the other two methods. For the TDDFT+TB and TDDFT results, the S_1 state arises from a σ_g to σ_u transition, while in TDDFT-aas, the S_1 state shows σ_g to π_u transitions. However, if α is 0.1, the optimized excitation energy is 1.88 eV, and the corresponding transition arises from σ_g to σ_u. The results indicate that modifying the α value will change the order of the excitation in Li_2. Thus, tuning the α value may be helpful for systems of interest.

In addition to diatomic molecules, the emission energies for the Thiel test set [32] of organic molecules were examined using the TDDFT-aas method. The optimizations were performed at the PBE/TZP level of theory. The emission energy differences between TDDFT-aas, TDDFT+TB, and TDDFT are shown in Figure 6 and Table S2.

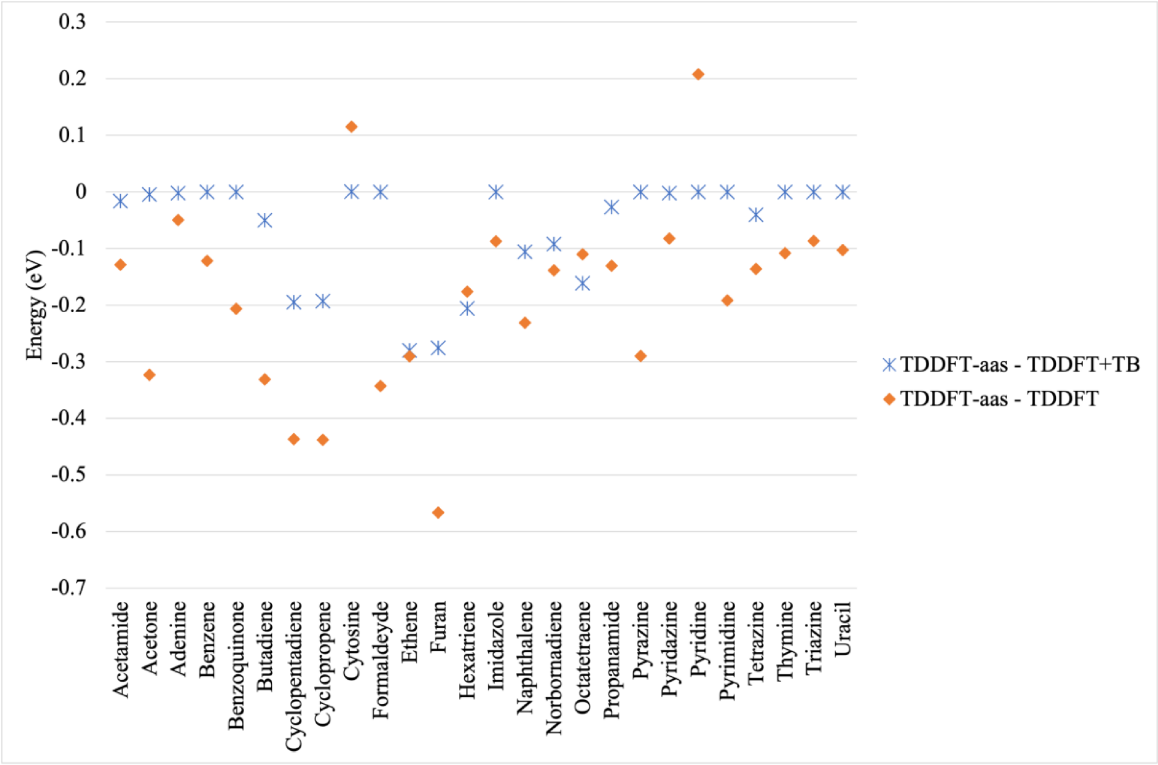

Figure 6 Emission energy differences among TDDFT-aas, TDDFT+TB, and TDDFT for organic molecules from the Thiel test set.

In general, the energy differences between TDDFT-aas and TDDFT+TB range from 0.00 to 0.29 eV, with both methods calculating the same optimized S_1 energy for many molecules. The similarity of these two methods is not surprising because the differences between the TDDFT-aas and TDDFT+TB gradient equations only arise in the fourth and fifth terms of equation 6. Ethene shows the highest energy difference between the TDDFT-aas and TDDFT+TB results at 0.29 eV. These results indicate that choosing 0.2 as the α value may still be reasonable for organic molecules.

For most systems, the agreement between TDDFT and TDDFT-aas is reasonable, ranging from 0.05 eV to 0.56 eV. However, a few cases occur that need further discussion. Furan shows the highest energy difference between TDDFT and TDDFT-aas. For the furan system, when the optimizations started from the same initial geometry, the energy at the S_1 minimum is calculated to be 5.56 eV, 4.70 eV, and 4.98 eV for the TDDFT, TDDFT-aas, and TDDFT+TB calculations, respectively. However, if furan were reoptimized using the TDDFT method starting from the final TDDFT-aas or TDDFT+TB S_1 optimized structure, the energy at the S_1 minimum is calculated to be 5.27 eV. If the reverse process is performed and furan is reoptimized starting from the original TDDFT S_1 optimized structure, the S_1 excitation energy remains as 4.70 eV using the TDDFT-aas

method or 4.98 eV using the TDDFT+TB method. For furan, TDDFT shows two optimized S_1 minima (corresponding to different excitation origins), whereas we have only been able to find one minimum point for TDDFT-aas and TDDFT+TB thus far.

For pyridazine, when the optimizations started from the same initial geometry, the energy at the S_1 minimum is calculated to be 1.71 eV, 2.27 eV, and 2.27 eV for the TDDFT, TDDFT-aas, and TDDFT+TB calculations, respectively. However, if the pyridazine were re-optimized starting from the TDDFT final optimized structure, the energy at the S_1 minimum is now calculated to be 1.63 eV for both TDDFT-aas and TDDFT+TB calculations. If the reverse process was performed and pyridazine was reoptimized starting from the TDDFT-aas or TDDFT+TB final optimized structure using the TDDFT method, the first excited state energy minimum is still calculated to be 1.71 eV. For pyridazine, TDDFT-aas and TDDFT+TB show two minimum points on the S_1 state surface, while TDDFT shows only one minimum point.

For tetrazine, when the optimizations started from the same initial geometry the energy at the S_1 minimum is calculated to be 2.28 eV, 3.06 eV, and 3.06 eV for the TDDFT, TDDFT-aas, and TDDFT+TB calculations, respectively. When tetrazine was reoptimized starting from the TDDFT final optimized structure, the energy at the S_1 minimum is now calculated to be 2.14 eV and 2.18 eV for TDDFT-aas and TDDFT+TB, respectively, which is quite close to the 2.28 eV calculated by TDDFT. If the reverse process is performed and tetrazine is reoptimized starting from the TDDFT-aas or TDDFT+TB final optimized structure using the TDDFT method, the energy at the S_1 minimum is now calculated to be 2.43 eV, which is a higher energy S_1 minimum. Thus for tetrazine, TDDFT-aas, TDDFT+TB, and TDDFT can find two excited state minima depending on the starting geometry; the initial minimum found is sensitive to the PES.

For the S_1 minimum state for ethene, the emission energies are calculated to be 5.58 eV, 6.71 eV, and 6.75 eV for the TDDFT-aas, TDDFT+TB, and TDDFT methods, respectively. For the electronic transition in the S_1 state, TDDFT-aas predicts that the π_u to π_g transition is responsible, whereas TDDFT+TB and TDDFT show that this state arises from the π_u to σ_u transition. When ethene was reoptimized starting from the TDDFT final optimized structure, the energy at the S_1 minimum is now calculated to be 5.58 eV and 6.73 eV for TDDFT-aas and TDDFT+TB, respectively. When ethene was reoptimized starting from the TDDFT-aas final optimized structure, the energy at the S_1 minimum is now calculated to be 5.89 eV for TDDFT+TB

and 6.17 eV for TDDFT. The results suggest that a second minimum may be possible for each method.

The results for the diatomic molecules and organic molecules indicated that TDDFT-aas shows good agreement with TDDFT+TB and TDDFT for most molecules. However, complications can arise when the excited state crosses or comes close to other excited states, and this can cause the excitation energy difference to be large between different computational methods. In addition, different initial geometries could find different minima for some organic molecules, depending on the system. In general, TDDFT has difficulty with state crossings. [33]

Finally, we examine the emission energies for two gold nanoclusters at the PBE/DZ level of theory; the results are shown in Table 4. For the gold clusters, the TDDFT-aas emission energy results show good agreement with TDDFT+TB and TDDFT, with energy differences within 0.03 eV. To examine the effects of the α parameter, for the $Au_{25}(SCH_2CH_2CH_3)_{18}^{-1}$ cluster calculations, α was set to 0.1 and 0.3 respectively to carry out the calculations again, and the emission energy results are 0.754 eV and 0.758 eV, respectively. The results indicate that α will slightly affect the results, but the general trends show that TDDFT-aas will very slightly underestimate the energy compared with TDDFT.

Table 4. Emission energy differences between TDDFT and TDDFT+TB for the gold nanoclusters.

	TDDFT-aas	**TDDFT+TB**	**TDDFT**
$Au_{25}(SCH_2CH_2CH_3)_{18}^{-1}$	0.75	0.76	0.77
Au_7^{+3}	1.90	1.91	1.93
$Au_{14}Cd(S\text{-}Adm)_{12}$	1.09	1.08	1.10

Comparison between computational cost

In this section, we examine the efficiency of the TDDFT-aas code. First, we compare the computational cost between TDDFT-aas, TDDFT+TB, and TDDFT energy calculations (Table 5). For the uracil molecule, TDDFT-aas and TDDFT+TB show the same computational cost, which is sped up by around a factor of 4.3 compared with TDDFT. For the metal nanoclusters, both TDDFT-aas and TDDFT+TB finished energy calculations within 70 minutes; meanwhile, TDDFT needs more than 20 hours to finish using the same number of cores.

Table 5. Comparison between the computational time (minutes) for TDDFT-aas, TDDFT+TB and TDDFT energy calculations. Most of the systems were computed using 8 cores; Ag_{116} and Ag_{120} were computed using 16 cores.

	TDDFT-aas	**TDDFT+TB**	**TDDFT**
uracil	0.17	0.17	0.73
Ag_{38}^{+4}	8.08	9.17	877.93
Au_{38}^{+4}	12.70	13.03	1544.75
Ag_{55}^{+5}	15.95	13.61	1311.25
Au_{55}^{+5}	39.03	34.98	638.50
$Au_{25}(SCH_3)_{18}^{-}$	6.05	6.39	362.23
Ag_{116}	63.54	62.26	4475.06
Ag_{120}	67.36	65.80	4700.79

We then examined the efficiency of the gradient calculations. The results for selected organic molecules and nanocluster systems are shown in Table 6 and Table 7, respectively (8 cores are used for all calculations).

Table 6. Comparison between the computational time (minutes) for TDDFT-aas, TDDFT+TB and TDDFT gradient calculations for three organic systems.

uracil	**TDDFT-aas**	**TDDFT+TB**	**TDDFT**
Computational time	1.1	1.1	5.2
Steps required to converge	6	6	6
furan	**TDDFT-aas**	**TDDFT+TB**	**TDDFT**
Computational time	0.52	0.53	2.65
Steps required to converge	5	5	4
ethene	**TDDFT-aas**	**TDDFT+TB**	**TDDFT**
Computational time	0.33	0.26	0.68
Steps required to converge	5	5	5
dibenzonaphthyridindione[a]	**TDDFT-aas**	**TDDFT+TB**	**TDDFT**
Computational time	5.40	5.33	21.72
Steps required to converge	5	5	5

[a]Coordinates obtained from Ref. [34]; structure 2 in the benchmark test.

Table 7. Comparison between the computational time (minutes) for TDDFT-aas, TDDFT+TB and TDDFT gradient calculations for gold clusters.

$Au_{25}(SCH_2CH_2CH_3)_{18}^{-1}$	**TDDFT-aas**	**TDDFT+TB**	**TDDFT**
Computational time	2098.48	1988.10	2604.37

Steps required to converge	56	53	50
Au_7^{3+}	**TDDFT-aas**	**TDDFT+TB**	**TDDFT**
Computational time	4.85	7.09	21.57
Steps required to converge	11	17	22
$Au_{14}Cd(S\text{-}Adm)_{12}$	**TDDFT-aas**	**TDDFT+TB**	**TDDFT**
Computational time	1740.10	1859.80	3075.74
Steps required to converge	38	41	40

For the organic systems, all three methods require similar numbers of steps to converge the geometries; TDDFT-aas can speed up the calculation by an average factor of 4.1 compared with TDDFT. The time savings is similar to TDDFT+TB. For $Au_{25}(SCH_2CH_2CH_3)_{18}^{-1}$, TDDFT-aas needs slightly more steps to converge the geometry compared with the other two methods. For Au_7^{3+} and $Au_{14}Cd(S\text{-}Adm)_{12}$, TDDFT-aas requires fewer steps to converge compare with TDDFT+TB and TDDFT and can reduce the computational cost. For the gradient calculation, TDDFT-aas and TDDFT+TB still reduce the computational cost, but not as significantly compared with energy calculations. Our evaluation shows that most of the computational costs are attributed to the calculation of the $\frac{dS_{\mu\nu}^{1/2}}{dR_A}$ term when solving the gradient equation. Improving the efficiency of the code is one of the directions for our future work.

Discussion

In summary, TDDFT-aas resembles the TDDFT-as method and the TDDFT+TB method: when solving the *K* coupling integrals in the excited state, an approximation is made instead of calculating the exact two-electron integrals. TDDFT-aas utilizes the γ_{AB} function from the TDDFT-as method via $K_{ia,jb} = \sum_{AB} q_{ia,A}\gamma_{AB}q_{jb,B}$ to calculate the coupling matrix. Because the γ_{AB} function is independent of tight binding parameters, TDDFT-aas will be easier to implement in codes that do not have tight binding parameters compared with TDDFT+TB. The performance of the TDDFT-aas method shows good agreement with TDDFT+TB and TDDFT, specifically for the metal nanocluster systems. For diatomic molecules and organic molecules, TDDFT-aas does not agree very well with TDDFT if state crossings are important. One option for excited state optimization in AMS is to use the eigenvector following method [35] when performing gradient calculations; however, the eigenvector following technique assumes the orbitals remain unchanged

during the process, which will not necessarily hold. These types of systems should employ the standard TDDFT method or more advanced multireference methods. Overall, TDDFT-aas shares similar characteristics and considerations with TDDFT+TB: (1) As shown in equation 5, $\mathbf{A} - \mathbf{B}$ is a diagonal matrix, so the methods are currently available for pure functionals; sTDDFT [10] is an alternative option if a hybrid functional calculation is expected. At the same time, since the approximation for the $\mathbf{A} - \mathbf{B}$ matrix violates the sum rule, both TDDFT+TB and TDDFT-aas have issues when predicting the oscillator strength for the excitation. (2) When approximating the coupling matrix, the monopole approximation is made, which leads to the issue that the atomic transition charges do not receive contributions from different atomic basis functions even if they are located on the same atom; for example, local excitations such as the σ_u to π_g transition in N_2 system are not treated correctly. [13] It has been reported that doing an on-site correction to the TD-DFTB method [36] and sTDDFT method [37] can improve the excitation energy results compared with TDDFT. Therefore, implementing an on-site correction to the current TDDFT+TB and TDDFT-aas methods may improve the local excitations such as the σ_u to π_g transition in the N_2 system as well.

Conclusion

In this work, we implemented both the energy and gradient of the TDDFT-aas method. The TDDFT-aas method starts with a standard ground state DFT calculation to determine the density as well as the Kohn-Sham orbitals and orbital energies, and then approximates the two-electron integral terms when solving the Casida equations. When approximating the two- electron integrals, calculation of the K coupling matrix uses a formula that involves γ_{AB} and atomic transition charges. Compared with TDDFT+TB, γ_{AB} in TDDFT-aas is not dependent on tight-binding parameters such as chemical hardness. We found that the exponent (α) can be set to be 0.2 for most of the systems in the benchmark test set, which ranges from diatomic molecules, organic molecules, and gold nanoclusters. The absorption spectra and emission energy results indicate that TDDFT-aas will give similar results to TDDFT+TB, and they share similar computational costs. Overall, TDDFT-aas opens a new way to approximate the TDDFT method without using tight-binding parameters to calculate chemical systems, and the method shows good agreement with TDDFT results, specifically for gold and silver nanoclusters.

Supplementary Material

Supplementary Material includes stick spectra of Au_{38}^{+4} and Au_{55}^{+5} calculated using TDDFT and TDDFT-aas; BP86 calculated results of spectra using TDDFT-aas, TDDFT+TB and TDDFT for the $Au_{25}(SCH_3)_{18}^{-}$ system; emission energy and the differences between TDDFT-aas, TDDFT+TB and TDDFT for diatomic molecules and organic molecules.

Acknowledgment

Y. W. and C.M.A. were supported by the National Science Foundation (Grant No. CHE-1955823) of the United States. The computing for this work was performed on the Beocat Research Cluster at Kansas State University, which is partially funded by the NSF (Grant Nos. CHE-1726332, CNS-1006860, EPS-1006860, and EPS-0919443). The authors thank Prof. Shane Parker for conversations that inspired this research. The authors thank Erik van Lenthe for help merging the codes into AMS.

Conflicts

The authors have no conflicts to disclose.

References

[1] C. Adamo and D. Jacquemin, *The Calculations of Excited-State Properties with Time-Dependent Density Functional Theory*, Chem. Soc. Rev. **42**, 845 (2013).

[2] A. Dreuw and M. Head-Gordon, *Single-Reference Ab Initio Methods for the Calculation of Excited States of Large Molecules*, Chem. Rev. **105**, 4009 (2005).

[3] A. D. Laurent and D. Jacquemin, *TD-DFT Benchmarks: A Review*, Int. J. Quantum Chem **113**, 2019 (2013).

[4] Y.-M. Byun, J. Sun, and C. A. Ullrich, *Time-Dependent Density-Functional Theory for Periodic Solids: Assessment of Excitonic Exchange–Correlation Kernels*, Electron. Struct. **2**, 023002 (2020).

[5] E. Runge and E. K. U. Gross, *Density-Functional Theory for Time-Dependent Systems*, Phys. Rev. Lett. **52**, 997 (1984).

[6] M. E. Casida, *Time-Dependent Density Functional Response Theory for Molecules*, in *Recent Advances in Computational Chemistry*, Vol. 1 (WORLD SCIENTIFIC, 1995), pp. 155–192.

[7] M. E. Casida and M. Huix-Rotllant, *Progress in Time-Dependent Density-Functional Theory*, Annu. Rev. Phys. Chem. **63**, 287 (2012).

[8] T. A. Niehaus, S. Suhai, F. Della Sala, P. Lugli, M. Elstner, G. Seifert, and Th. Frauenheim, *Tight-Binding Approach to Time-Dependent Density-Functional Response Theory*, Phys. Rev. B **63**, 085108 (2001).
[9] F. Trani, G. Scalmani, G. Zheng, I. Carnimeo, M. J. Frisch, and V. Barone, *Time-Dependent Density Functional Tight Binding: New Formulation and Benchmark of Excited States*, J. Chem. Theory Comput. **7**, 3304 (2011).
[10] C. Bannwarth and S. Grimme, *A Simplified Time-Dependent Density Functional Theory Approach for Electronic Ultraviolet and Circular Dichroism Spectra of Very Large Molecules*, Computational and Theoretical Chemistry **1040–1041**, 45 (2014).
[11] S. Grimme, *A Simplified Tamm-Dancoff Density Functional Approach for the Electronic Excitation Spectra of Very Large Molecules*, J. Chem. Phys. **138**, 244104 (2013).
[12] T. Risthaus, A. Hansen, and S. Grimme, *Excited States Using the Simplified Tamm–Dancoff-Approach for Range-Separated Hybrid Density Functionals: Development and Application*, Phys. Chem. Chem. Phys. **16**, 14408 (2014).
[13] R. Rüger, E. Van Lenthe, T. Heine, and L. Visscher, *Tight-Binding Approximations to Time-Dependent Density Functional Theory — A Fast Approach for the Calculation of Electronically Excited States*, J. Chem. Phys. **144**, 184103 (2016).
[14] G. Giannone and F. Della Sala, *Minimal Auxiliary Basis Set for Time-Dependent Density Functional Theory and Comparison with Tight-Binding Approximations: Application to Silver Nanoparticles*, J. Chem. Phys. **153**, 084110 (2020).
[15] Z. Zhou, F. Della Sala, and S. M. Parker, *Minimal Auxiliary Basis Set Approach for the Electronic Excitation Spectra of Organic Molecules*, J. Phys. Chem. Lett. **14**, 1968 (2023).
[16] O. Baseggio, G. Fronzoni, and M. Stener, *A New Time Dependent Density Functional Algorithm for Large Systems and Plasmons in Metal Clusters*, The Journal of Chemical Physics **143**, 024106 (2015).
[17] D. Porezag, Th. Frauenheim, Th. Köhler, G. Seifert, and R. Kaschner, *Construction of Tight-Binding-like Potentials on the Basis of Density-Functional Theory: Application to Carbon*, Phys. Rev. B **51**, 12947 (1995).
[18] G. Seifert, D. Porezag, and Th. Frauenheim, *Calculations of Molecules, Clusters, and Solids with a Simplified LCAO-DFT-LDA Scheme*, Int. J. Quantum Chem. **58**, 185 (1996).
[19] N. Asadi-Aghbolaghi, R. Rüger, Z. Jamshidi, and L. Visscher, *TD-DFT+TB: An Efficient and Fast Approach for Quantum Plasmonic Excitations*, J. Phys. Chem. C **124**, 7946 (2020).
[20] S. Havenridge and C. M. Aikens, *Deciphering the Dual Emission in the Photoluminescence of $Au_{14}Cd(SR)_{12}$: A Theoretical Study Using TDDFT and TDDFT + TB*, J. Chem. Phys. **155**, 074302 (2021).
[21] A. Baghdasaryan, C. Besnard, L. M. Lawson Daku, T. Delgado, and T. Burgi, *Thiolato Protected Copper Sulfide Cluster with the Tentative Composition $Cu_{74}S_{15}(2\text{-}PET)_{45}$*, Inorg. Chem. **59**, 2200 (2020).
[22] J. Sun et al., *Labile Ligands Protected Cu_{50} Nanoclusters with Tailorable Optical Limiting Effect*, ACS Materials Lett. **6**, 281 (2024).
[23] P. D'Antoni, M. Medves, D. Toffoli, A. Fortunelli, M. Stener, and L. Visscher, *A Resolution of Identity Technique to Speed up TDDFT with Hybrid Functionals: Implementation and Application to the Magic Cluster Series $Au_{8n+4}(SC_6H_5)_{4n+8}$ (n = 3–6)*, J. Phys. Chem. A **127**, 9244 (2023).

[24] M. Monti, M. F. Matus, S. Malola, A. Fortunelli, M. Aschi, M. Stener, and H. Häkkinen, *What Contributes to the Measured Chiral Optical Response of the Glutathione-Protected Au_{25} Nanocluster?*, ACS Nano **17**, 11481 (2023).
[25] S. Havenridge, R. Rüger, and C. M. Aikens, *Analytical Excited State Gradients for Time-Dependent Density Functional Theory plus Tight Binding (TDDFT + TB)*, J. Chem. Phys. **158**, 224103 (2023).
[26] G. te Velde, F. M. Bickelhaupt, E. J. Baerends, C. Fonseca Guerra, S. J. A. van Gisbergen, J. G. Snijders, and T. Ziegler, *Chemistry with ADF*, J. Comput. Chem. **22**, 931 (2001).
[27] J. P. Perdew, K. Burke, and M. Ernzerhof, *Generalized Gradient Approximation Made Simple*, Phys. Rev. Lett. **77**, 3865 (1996).
[28] E. Van Lenthe and E. J. Baerends, *Optimized Slater-type Basis Sets for the Elements 1–118*, J Comput Chem **24**, 1142 (2003).
[29] J. P. Perdew, *Density-Functional Approximation for the Correlation Energy of the Inhomogeneous Electron Gas*, Phys. Rev. B **33**, 8822 (1986).
[30] A. D. Becke, *Density-Functional Exchange-Energy Approximation with Correct Asymptotic Behavior*, Phys. Rev. A **38**, 3098 (1988).
[31] W. Kolos and C. C. J. Roothaan, *Accurate Electronic Wave Functions for the H_2 Molecule*, Rev. Mod. Phys. **32**, 219 (1960).
[32] M. Schreiber, M. R. Silva-Junior, S. P. A. Sauer, and W. Thiel, *Benchmarks for Electronically Excited States: CASPT2, CC2, CCSD, and CC3*, J. Chem. Phys. **128**, 134110 (2008).
[33] M. Barbatti and R. Crespo-Otero, *Surface Hopping Dynamics with DFT Excited States*, in *Density-Functional Methods for Excited States*, edited by N. Ferré, M. Filatov, and M. Huix-Rotllant, Vol. 368 (Springer International Publishing, Cham, 2014), pp. 415–444.
[34] S. Tussupbayev, N. Govind, K. Lopata, and C. J. Cramer, *Comparison of Real-Time and Linear-Response Time-Dependent Density Functional Theories for Molecular Chromophores Ranging from Sparse to High Densities of States*, J. Chem. Theory Comput. **11**, 1102 (2015).
[35] *Https://Www.Scm.Com/Doc/ADF/Input/Excited_state_optimizations.Html*, (unpublished).
[36] A. Domínguez, B. Aradi, T. Frauenheim, V. Lutsker, and T. A. Niehaus, *Extensions of the Time-Dependent Density Functional Based Tight-Binding Approach*, J. Chem. Theory Comput. **9**, 4901 (2013).
[37] M. De Wergifosse and S. Grimme, The eXact Integral Simplified Time-Dependent Density Functional Theory (XsTD-DFT), preprint, Chemistry, 2024.